Journal of Quantitative Spectroscopy & Radiative Transfer 113 (2012) 749–762

Contents lists available at SciVerse ScienceDirect

Journal of Quantitative Spectroscopy & Radiative Transfer

journal homepage: www.elsevier.com/locate/jqsrt

High sensitivity CW-Cavity Ring Down Spectroscopy of N_2O between 6950 and 7653 cm^{-1} (1.44–1.31 μm): I. Line positions

Y. Lu [a,b], D. Mondelain [a], A.W. Liu [b], V.I. Perevalov [c], S. Kassi [a], A. Campargue [a,*]

[a] Université Grenoble 1/CNRS, UMR5588 LIPhy, Grenoble F-38041, France
[b] Hefei National Laboratory for Physical Sciences at Microscale, Department of Chemical Physics, University of Science and Technology of China, Hefei 230026, China
[c] Laboratory of Theoretical Spectroscopy, V.E. Zuev Institute of Atmospheric Optics SB, Russian Academy of Science, 1 Akademician Zuev sq., 634021 Tomsk, Russia

ARTICLE INFO

Article history:
Received 13 January 2012
Received in revised form
29 February 2012
Accepted 2 March 2012
Available online 10 March 2012

Keywords:
Nitrous oxide
N_2O
Isotopologue
CRDS
Effective Hamiltonian

ABSTRACT

The absorption spectrum of nitrous oxide, N_2O, has been recorded by CW-Cavity Ring Down Spectroscopy between 6950 and 7653 cm^{-1}. The spectra were obtained at Doppler limited resolution using a CW-CRDS spectrometer based on a series of fibered DFB laser diodes. The typical noise equivalent absorption, in the order of $\alpha_{min} \approx 1 \times 10^{-10}$ cm^{-1}, allowed for the detection of lines with intensity as small as 1×10^{-29} cm/molecule.

The positions of 7203 lines of four isotopologues ($^{14}N_2{}^{16}O$, $^{14}N^{15}N^{16}O$, $^{15}N^{14}N^{16}O$ and $^{14}N_2{}^{18}O$) were measured with a typical accuracy of 1.0×10^{-3} cm^{-1}. The transitions were rovibrationally assigned on the basis of the global effective Hamiltonian models developed for each isotopologue. The band by band analysis allowed for the determination of the rovibrational parameters of more than 95 bands, most of them being newly reported while new rotational transitions are measured for the others. The measured line positions of the main isotopologue are found to be in good agreement with the predictions of the effective Hamiltonian model but a few deviations up to 0.20 cm^{-1} are observed. Local rovibrational perturbations were evidenced for several bands. The interaction mechanisms and the perturbers were univocally assigned on the basis of the effective Hamiltonian models.

1. Introduction

The present contribution is the fifth of a series devoted to the study of the near infrared absorption spectrum of nitrous oxide by CW-Cavity Ring Down Spectroscopy (CW-CRDS). [1–4]. Compared to the previous investigations by Fourier Transform spectroscopy (FTS) [5–8] associated with long multipass cells, the very high sensitivity of the CRDS technique allowed lowering the detectivity threshold by about three orders of magnitude leading to the observation of many new bands. Using a set of about seventy Distributed Feed-Back (DFB) laser diodes, the 5905–7920 cm^{-1} range was continuously covered with a typical noise equivalent absorption of $\alpha_{min} \approx 1 \times 10^{-10}$ cm^{-1}. For instance, in the 5905–7066 cm^{-1} region, a total of about 10,500 transitions belonging to 132 bands of five N_2O isotopologues were reported [1–3]. In the present work, we fill the gap between Refs. [1–3] (5905–7066 cm^{-1}) and Ref. [4] (7647–7918 cm^{-1}) by the study of the 6950–7653 cm^{-1} interval (see Fig. 1 of Ref. [4]). More than 8000 lines involving the four most abundant isotopologues ($^{14}N_2{}^{16}O$, $^{15}N^{14}N^{16}O$, $^{14}N^{15}N^{16}O$ and $^{14}N_2{}^{18}O$) were detected. In the following, we present the rovibrational assignment of the spectrum performed on the basis of the predictions of the effective Hamiltonian models developed for each isotopologue [9–11], and the sets of the spectroscopic parameters derived from the band by band analysis.

* Corresponding author.
E-mail address: Alain.Campargue@ujf-grenoble.fr (A. Campargue).

0022-4073/$ - see front matter © 2012 Elsevier Ltd. All rights reserved.
doi:10.1016/j.jqsrt.2012.03.005

2. Experiment

2.1. The CW-CRDS spectrometer

The fibered Distributed Feed-Back diode laser CW-CRDS spectrometer was described in details in Refs. [12–14]. Each DFB diode laser has a typical tuning range of 7 nm ($\sim$35 cm^{-1}) by temperature tuning from -15 to 60 °C. Twenty four diode lasers were necessary to cover continuously the 6950–7653 cm^{-1} region. A single-mode fiber delivers the laser radiation to one end of a vacuum-tight ringdown cell, which is 140 cm long. The high reflectivity cavity mirrors are mounted on tilt stages, one of which includes a piezoelectric tube. The cavity losses at each laser wavelength were obtained by averaging the results of exponential fits of about 35 ringdown events, thus giving one data point in the spectrum. Ringdown time values ranged between 90 and 220 μs. About 60 min were needed for each DFB laser in order to complete a temperature scan.

The pressure, measured by a capacitance gauge (Baratron), as well as the ringdown cell temperature (294.6 ± 0.3 K) were continuously monitored during the recordings. The spectra were obtained at pressure of 10.0 Torr. Additional recordings were performed at 2.00 Torr in the regions corresponding to the strongest lines which were sometimes too absorptive at 10 Torr.

The wavenumber calibration of the spectra was based on the values provided by a lambdameter (Burleigh WA1650). It was then refined using line positions of H_2O present as an impurity in the cell. Their values were taken from the HITRAN database [15]. The maximum differences between line positions measured on the overlapping part of two successive spectra are less than of 2×10^{-3} cm^{-1}. We then estimate to 1×10^{-3} cm^{-1} the average uncertainty on the line positions.

The sensitivity and high signal to noise ratio of the CRDS spectra are illustrated in Fig. 1. A noise equivalent absorption on the order of $\alpha_{min} \approx 1 \times 10^{-10}$ cm^{-1} was achieved. It led to the observation of a large number of lines involving many hot bands of the main isotopologue ($^{14}N_2{}^{16}O$) and the contribution of three minor isotopologues ($^{15}N^{14}N^{16}O$, $^{14}N^{15}N^{16}O$ and $^{14}N_2{}^{18}O$) in "natural" isotopic abundance. As an example,

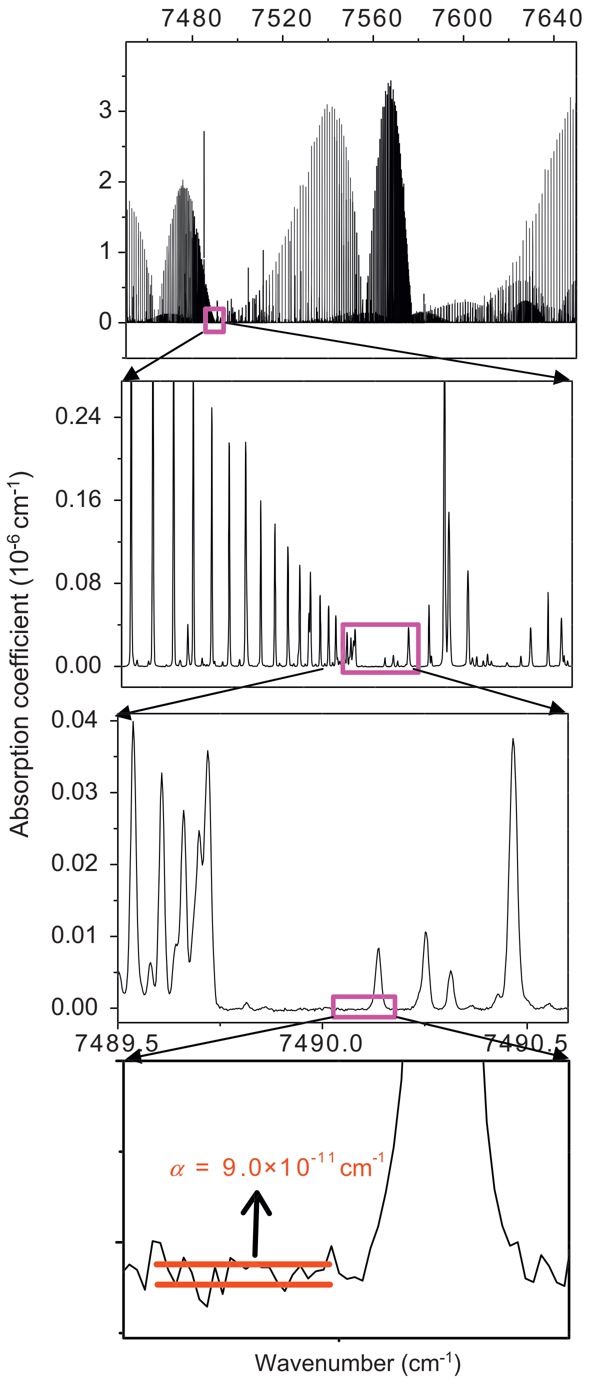

Fig. 1. CW-CRDS spectrum of N_2O near 7560 cm^{-1}. The sample pressure was 10.0 Torr. Four successive enlargements illustrate the high dynamics achieved by the CW-CRDS spectrometer allowing for the measurement of absorption coefficient differing by four orders of magnitude, from 3×10^{-6} cm^{-1} to the noise level at about 1×10^{-10} cm^{-1}.

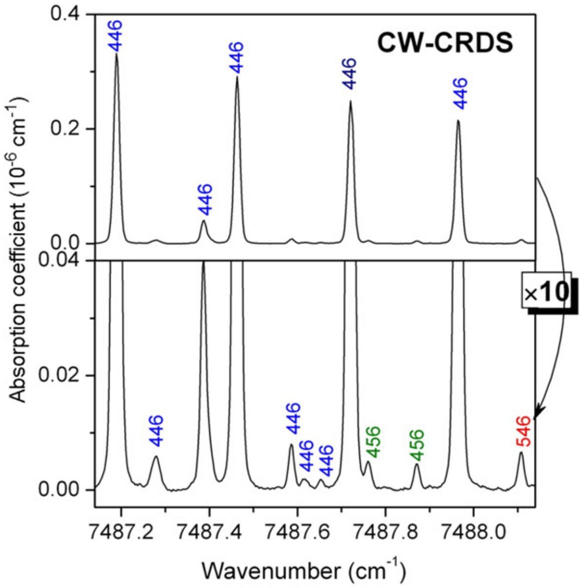

Fig. 2. Small section of the CW-CRDS spectrum of N_2O near 7488 cm^{-1} showing twelve transitions belonging to three isotopologues: $^{14}N_2{}^{16}O$ (446), $^{15}N^{14}N^{16}O$ (546) and $^{14}N^{15}N^{16}O$ (456).

Table 1
Summary of the line position measurements for the different isotopologues of N_2O between 6950 and 7653 cm^{-1}.

Isotopologue	HITRAN notation	Abundance [17]	Number of bands			Number of transitions
			This work	Literature[a]	HITRAN	
$^{14}N_2{}^{16}O$	446	0.990333	71	14	2	5912
$^{14}N^{15}N^{16}O$	456	3.64093×10^{-3}	9[b]	10	0	544
$^{15}N^{14}N^{16}O$	546	3.64093×10^{-3}	10[c]	9	0	525
$^{14}N_2{}^{18}O$	448	1.98582×10^{-3}	5	0	0	222
Total			95	33	2	7203

[a] Literature data sources are the following: $^{14}N_2{}^{16}O$: Refs. [5–8,18], $^{14}N^{15}N^{16}O$ [19], $^{15}N^{14}N^{16}O$ [23].
[b] Including the newly observed 5200–0000 band ((12 0 14)–(001)) at 7384.081 cm^{-1}. Ref. [19] includes a Π–Σ band at 6981.85 cm^{-1} and a Π–Π band at 7039.72 cm^{-1} for which only a few transitions were observed in the present CRDS spectrum of "natural" N_2O.
[c] Including the 5200–0000 band at 7275.900 cm^{-1} ((12 0 13)–(001)) and a Π–Π band at 7543.012 cm^{-1}, newly observed. Ref. [20] includes a Π–Π band at 7056.44 cm^{-1} for which only a few transitions were observed in the present CRDS spectrum of "natural" N_2O.

Table 2
Vibrational assignment and fractions respective to the basis states for the bands of $^{14}N_2{}^{16}O$, $^{14}N^{15}N^{16}O$, $^{15}N^{14}N^{16}O$ and $^{14}N_2{}^{18}O$ observed by CW-CRDS between 6950 and 7653 cm^{-1}.

ΔP	Band[a]	(P, l_2, i)[b]	ΔG_v (cm^{-1})	G_v (cm^{-1})	Basis states[c]	% Fraction[d]
$^{14}N_2{}^{16}O$ cold bands						
12	3201–0000	(12 0 8)	7024.093	7024.093	$32^01/16^01/08^01$	34/25/21
12	3600–0000	(12 0 9)	7029.843	7029.843	$36^00/0(12)^00/44^00/1(10)^00$	30/26/22/18
12	3221–0000	(12 2 15)	7037.174	7037.174	$32^21/16^21$	26/23
13	0113–0000	(13 1 1)	7126.979	7126.979	01^13	98
12	4001–0000	(12 0 10)	7137.127	7137.127	$40^01/24^01/16^01$	39/21/20
12	2421–0000	(12 2 18)	7162.659	7162.659	$24^21/32^21/16^21$	38/28/20
13	0512–0000	(13 1 2)	7179.330	7179.330	$05^12/13^12$	59/35
12	0(12)00–0000	(12 0 11)	7194.365	7194.365	$0(12)^00/44^00/28^00/52^00$	31/26/22/18
12	3201–0000	(12 0 12)	7214.679	7214.679	$32^01/40^01/24^01$	29/28/19
13	0512–0000	(13 1 4)	7325.612	7325.612	$05^12/21^12/13^12$	34/31/30
12	5200–0000	(12 0 13)	7340.792	7340.792	$52^00/0(12)^00/36^00/$	32/20/20
12	5220–0000	(12 2 23)	7355.032	7355.032	$52^20/36^20/0(12)^20/1(10)^20$	34/21/20/17
13	2112–0000	(13 1 7)	7443.004	7443.004	$21^12/13^12$	54/29
12	6000–0000	(12 0 14)	7463.985	7463.985	$60^00/44^00/1(10)^00$	31/19/19
12	5220–0000	(12 2 25)	7488.631	7488.631	$52^20/1(10)^20/44^20$	33/22/17
12	6000–0000	(12 0 15)	7556.135	7556.135	$60^00/52^00$	40/16
12	3620–0000	(12 2 27)	7610.617	7610.617	$36^20/28^20/44^20$	30/23/22
12	3600–0000	(12 0 16)	7640.474	7640.474	$36^00/44^00$	25/25
14	0203–0000	(14 0 1)	7665.273	7665.273	02^03	87
14	0223–0000	(14 2 2)	7673.636	7673.636	02^23	98
$^{14}N_2{}^{16}O$ hot bands						
12	0(10)01–0200	(14 0 10)	6977.420	8145.553	$0(10)^01/42^01$	26/22
12	0(10)21–0220	(14 2 20)	6977.665	8155.410	$0(10)^21/42^21$	19/18
12	1801–1000	(14 0 12)	6991.422	8276.325	$18^01/42^01/50^01$	22/19/17
12	0911–0110	(13 1 8)	7000.644	7589.412	$09^11/33^11/41^11/17^11$	24/22/16/16
12	4510–0110	(13 1 9)	7003.520	7592.289	$45^10/0(13)^10/37^10/1(11)^10$	25/21/20/19
13	0313–0200	(15 1 1)	7037.135	8205.268	$03^13/11^13$	80/17
13	0203–0110	(14 0 1)	7076.507	7665.275	02^03	87
13	0223–0110	(14 2 2)	7084.868	7673.635	02^23	98
12	5001–1000	(14 0 14)	7091.447	8376.350	$50^01/26^01$	37/16
12	5111–0310	(15 1 12)	7094.387	8843.452	$51^11/19^11/35^11/0(11)^11$	24/20/17/16
12	4331–0330	(15 3 22)	7106.188	8873.101	$43^31/19^31$	33/26
12	1801–0200	(14 0 12)	7108.193	8276.326	$18^01/42^01/50^01$	22/19/17
12	4221–0220	(14 2 22)	7116.376	8294.120	$42^21/18^21$	36/26
12	4111–0110	(13 1 10)	7126.296	7715.064	$41^11/17^11$	39/24
12	3401–1000	(14 0 15)	7167.733	8452.636	$34^01/42^01/26^01$	24/21/16
12	3511–1110	(15 1 16)	7181.075	9061.341	$35^11/43^11/27^11$	25/20/18
12	5001–0200	(14 0 14)	7208.218	8376.350	$50^01/26^01$	37/16
12	3311–0110	(13 1 12)	7229.065	7817.833	$33^11/25^11/41^11$	30/24/19
12	3421–0220	(14 2 26)	7237.061	8414.805	$34^21/26^21$	29/27
12	3401–0200	(14 0 15)	7284.504	8452.636	$34^01/42^01/26^01$	24/21/16
12	6200–0200	(14 0 16)	7307.591	8475.724	$62^00/0(14)^00$	25/25
12	0(14)20–0220	(14 2 29)	7310.114	8487.858	$0(14)^20/62^20/54^20$	25/21/17
12	5310–0110	(13 1 13)	7324.358	7913.126	$53^10/0(13)^10/61^10$	25/23/16
12	6200–1000	(14 0 17)	7328.046	8612.949	62^00	22
14	0114–1110	(17 1 1)	7365.814	9246.080	01^14	96
14	0004–1000	(16 0 1)	7429.237	8714.140	00^04	96

Table 2 (*continued*)

ΔP	Band[a]	(P, l_2, i)[b]	ΔG_v (cm^{-1})	G_v (cm^{-1})	Basis states[c]	% Fraction[d]
12	7000–1000	(14 0 18)	7440.197	8725.100	70^00	38
12	6200–0200	(14 0 17)	7444.816	8612.948	62^00	22
12	6220–0220	(14 2 31)	7453.387	8631.131	$62^20/1(12)^20$	35/18
14	0403–1000	(16 0 2)	7454.402	8739.306	$04^03/12^03$	68/27
12	6110–0110	(13 1 14)	7457.582	8046.350	$61^10/1(11)^10/45^10$	35/19/18
14	0533–0330	(17 3 3)	7522.100	9289.012	$05^33/13^33$	71/27
12	7000–1000	(14 0 19)	7525.859	8810.762	$70^00/62^00$	24/23
14	0513–0310	(17 1 2)	7526.077	9275.142	$05^13/13^13$	60/34
14	0004–0200	(16 0 1)	7546.008	8714.140	00^04	96
12	7000–0200	(14 0 18)	7556.967	8725.099	70^00	38
14	0423–0220	(16 2 3)	7568.846	8746.590	$04^23/12^23$	75/22
12	6110–0110	(13 1 15)	7570.894	8159.662	$61^10/53^10/29^10$	28/22/17
14	0403–0200	(16 0 2)	7571.173	8739.305	$04^03/12^03$	68/27
12	5420–0220	(14 2 33)	7582.350	8760.094	$54^20/62^20/1(12)^20/2(10)^20$	24/21/18/16
14	1203–1000	(16 0 4)	7592.136	8877.039	$12^03/04^03/20^03$	47/27/19
14	0313–0110	(15 1 1)	7616.500	8205.268	$03^13/11^13$	80/17
14	1443–0440	(18 4 12)	7637.137	9993.389	$14^43/06^43$	64/31
14	2113–1110	(17 1 7)	7656.988	9537.254	$21^13/13^13$	52/29
14	1004–0001	(18 0 4)	7664.800	9888.557	10^04	80
14	1333–0330	(17 3 7)	7674.098	9441.010	$13^33/05^33$	67/27
12	3710–0110	(13 1 16)	7677.516	8266.283	$37^10/45^10/29^10$	25/24/17
14	2003–1000	(16 0 7)	7691.585	8976.488	$20^03/12^03$	62/20
14	1203–0200	(16 0 4)	7708.909	8877.041	$12^03/04^03/20^03$	47/27/19
14	1223–0220	(16 2 7)	7710.775	8888.520	$12^23/04^23$	71/23
14	1113–0110	(15 1 3)	7747.029	8335.797	$11^13/03^13$	76/17
$^{14}N^{15}N^{16}O$						
12	2401–0000	(12 0 10)	7051.776	7051.776	$24^01/40^01$	33/30
12	4001–0000	(12 0 12)	7143.396	7143.396	$40^01/32^01$	57/28
12	4110–0110	(13 0 12)	7149.731	7725.165	$41^11/33^11$	42/35
12	5200–0000	(12 0 14)	7384.081	7384.081	$52^00/28^00/1(10)^00/60^00$	26/20/17/17
12	6000–0000	(12 0 15)	7492.122	7492.122	$60^00/36^00$	47/20
14	0203–0000	(14 0 1)	7511.637	7511.637	02^03	91
12	5200–0000	(12 0 16)	7567.429	7567.429	$52^00/60^00/44^00$	30/29/22
14	1113–0110	(15 1 3)	7614.998	8190.432	11^13	84
14	1003–0000	(14 0 3)	7650.754	7650.754	10^03	89
$^{15}N^{14}N^{16}O$						
12	3201–0000	(12 0 8)	6957.900	6957.900	$32^01/08^01/16^01$	34/24/20
12	4001–0000	(12 0 10)	7065.525	7065.525	$40^01/16^01/24^01$	47/21/16
12	3201–0000	(12 0 12)	7142.129	7142.129	$32^01/40^01/24^01$	32/25/24
12	5200–0000	(12 0 13)	7275.900	7275.900	$52^00/0(12)^00/36^00$	32/21/18
12	6000–0000	(12 0 14)	7394.271	7394.271	$60^00/44^00/1(10)^00$	39/19/18
12	6000–0000	(12 0 15)	7482.856	7482.856	$60^00/52^00$	38/22
14	0313–0110	(15 1 1)	7543.012	8128.324	$03^13/11^13$	75/20
14	0203–0000	(14 0 1)	7592.486	7592.486	02^03	84
14	1113–0110	(15 1 3)	7667.804	8253.116	$11^13/03^13$	72/22
14	1003–0000	(14 0 3)	7702.500	7702.500	10^03	81
$^{14}N_2{}^{18}O$						
12	4001–0000	(12 0 10)	7006.341	7006.341	$40^01/24^01$	60/26
12	6000–0000	(12 0 14)	7292.375	7292.375	$60^00/28^00$	42/19
12	6000–0000	(12 0 15)	7376.572	7376.572	$60^00/36^00/52^00$	44/20/18
14	0203–0000	(14 0 1)	7630.843	7630.843	02^03	91
14	1003–0000	(14 0 3)	7718.948	7718.948	10^03	91

[a] $v_1v_2l_2v_3$ corresponding to the maximum value of the modulo of the expansion coefficients of the eigenfunction. For clarity, v_2 values larger than 9 are written between parenthesis.
[b] Cluster labeling notation: ($P=2v_1+v_2+4v_3$, l, i) for the upper state of the band; i is the order number within the cluster increasing with the energy.
[c] Only basis states with modulo of expansion coefficients larger than 0.4 are presented.
[d] Squares of the expansion coefficients of the vibrational state for the dominant basis states appearing in the preceding column.

Fig. 2 shows a 1 cm^{-1} spectral section where twelve lines belonging to three isotopologues are detected. Lines due to impurities (water, CO_2 and HF) were identified using the corresponding HITRAN line list [15]. After removal of these impurity lines, a set of about 8000 lines was obtained. The average density of lines is then about 12/cm^{-1} which made the analysis particularly difficult.

3. Rovibrational analysis

3.1. Rovibrational assignment

A summary of the observations is presented in Table 1 which includes the HITRAN notation of the various isotopologue species and the corresponding

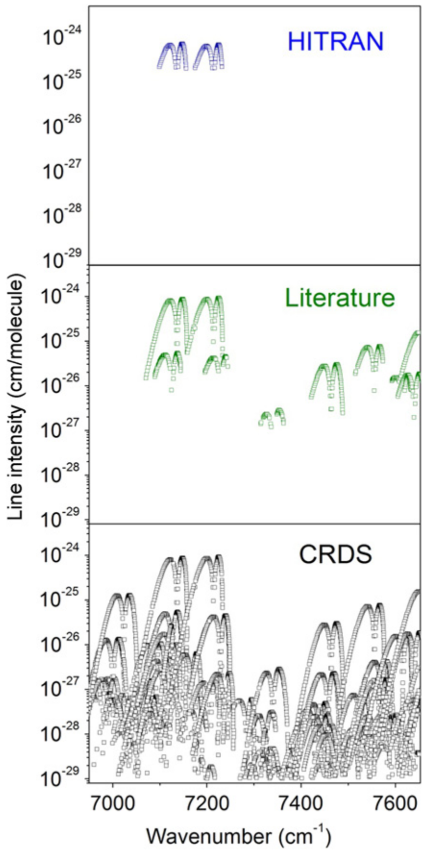

Fig. 3. Overview comparison of the CRDS observations of $^{14}N_2{}^{16}O$ transitions between 6950 and 7653 cm^{-1} with the list provided in the HITRAN database (upper panel) and the observations available in the literature [5–8,18] (middle panel). The line intensities of the two lower panels are approximate values which were calculated using the set of effective dipole moment parameters of Ref. [17] slightly refined using the eigenfunctions of the new effective Hamiltonian [9]. A logarithmic scale is used for the line intensities.

abundance. Overall, 7203 transitions were assigned on the basis of the predictions of the effective Hamiltonian (EH) of Ref. [16]. This rovibrational model is based on a polyad structure resulting from the approximate relations between the harmonic frequencies $\omega_3 \approx 2\omega_1 \approx 4\omega_2$. The EH parameters values have been fitted to the observed line positions for each isotopic species and can be found in the following references: $^{14}N_2{}^{16}O$ [9], $^{15}N^{14}N^{16}O$ [10], $^{14}N^{15}N^{16}O$ [10] and $^{14}N_2{}^{18}O$ [11]. As the mixing between the $(v_1 v_2^{l_2} v_3)$ states may be strong, the vibrational states are preferably labeled using the $(P=2v_1+v_2+4v_3, l_2, i)$ triplet where the index i increases with the energy. The absorption in the studied region corresponds to a $\Delta P=12$, 13 and 14 variation of the polyad quantum number (see Fig. 1 of Ref. [4]). The vibrational labellings and the dominant basis states in the vibrational decomposition of the upper states of the various bands are listed in Table 2. Note that the same $(v_1 v_2^{l_2} v_3)$ state may be dominant in the eigenfunction expansion of different vibrational states.

3.2. Band by band rotational analysis

In the case of unperturbed bands, the rotational analysis was performed using the standard equation for the vibration–rotation energy levels:

$$F_v(J) = G_v + B_v J(J+1) - D_v J^2(J+1)^2 + H_v J^3(J+1)^3, \quad (1)$$

where G_v is the vibrational term value, B_v is the rotational constant, D_v and H_v are centrifugal distortion constants. The spectroscopic parameters were fitted directly to the measured wavenumbers and, in the case of hot bands involving *e* and *f* rotational levels, the *ee*, *ef*, *fe* and *ff* sub bands were considered independently. The lower state rotational constants were constrained to their literature values [5]. The global line list provided as Supplementary material includes the deviations between the measured line positions and the values calculated with the fitted rovibrational parameters. In the case of bands located near the borders of the investigated region, the input data set was completed with the line positions measured by CRDS in the surrounding regions [3,4] (the added line positions are indicated in the Supplementary material).

3.2.1. $^{14}N_2{}^{16}O$

Overall, 5912 transitions belonging to seventy one bands were assigned to the main isotopologue. For comparison only 130 transitions of the $3\nu_1+2\nu_2+\nu_3$ and $4\nu_1+\nu_3$ bands measured by Toth [5] are included in the HITRAN line list. Fig. 3 shows an overview comparison of our measurements with the HITRAN line list and a compilation of the measurements available in the literature [5–8,18] (excluding our CRDS measurements below 7066 cm^{-1} [1–3] and above 7647 cm^{-1} [4]). The line intensities used in Fig. 3 for the CRDS and literature data were calculated using the set of effective dipole moment parameters of Ref. [17] which were slightly refined using the eigenfunctions of the new effective Hamiltonian [9]. Fig. 3 illustrates that the present results considerably extend the observations in the region. Among the 71 $^{14}N_2{}^{16}O$ bands presently analyzed, only 14 (corresponding to less than 800 line positions) were previously reported. Previous measurements in the region are due to Toth [5] (3 bands), Weirauch et al. [7] (8 bands), Wang et al. [8] (3 bands) who used FTS associated with a multipass cell (pathlength up to 433, 27.5 and 105 m, respectively). Five bands were also detected by Oshika et al. [18] using an external cavity diode laser. (Note that one additional band at 7650.75 cm^{-1} reported in Ref. [18] without vibrational assignment is in fact the $\nu_1+3\nu_3$ band of $^{14}N^{15}N^{16}O$ [19].)

The parameters retrieved from the fit of the line positions are listed in Table 3. The *rms* values of the (obs.−calc.) deviations are generally smaller than 1.0×10^{-3} cm^{-1} which is consistent with the uncertainty on the line positions. As marked in Table 3, several bands were found to be affected by a perturbation; the corresponding perturbed positions were excluded from the fit. The perturbations will be analyzed in the next Section. When available, previous determinations of band parameters have been included in Table 3 for comparison. The overall agreement is satisfactory and the significant increase of the maximum *J* values allowed

Table 3
Spectroscopic parameters (in cm^{-1}) of the rovibrational bands of $^{14}N_2{}^{16}O$ assigned for the CW-CRDS spectra between 6950 and 7653 cm^{-1}. The cold and hot bands are listed successively and ordered according to their ΔG_v values.

Lower states constants [5]

State $v_1v_2l_2v_3$	(P, l_2, i)	G_v	B_v	$D_v \times 10^7$	$H_v \times 10^{12}$
0000e	(0 0 1)	0.0	0.419 011 001	1.760919	−0.016529
0110*e*	(1 1 1)	588.76787	0.419 177 925	1.783245	−0.01714
0110f		588.76787	0.419 969 845	1.793030	−0.01766
0200e	(2 0 1)	1168.13230	0.419 920 952	2.491945	2.955393
0220e	(2 2 2)	1177.74467	0.420 125 256	1.196792	−2.950211
0220f		1177.74467	0.420 126 260	1.818000	0.095
1000e	(2 0 2)	1284.90334	0.417 255 210	1.726978	0.14666
0310e	(3 1 1)	1749.06523	0.419 583 944	2.110353	1.2225
0310f		1749.06515	0.421 079 073	2.177366	−0.35921
0330e	(3 3 2)	1766.91238	0.420 667 053	1.617863	−0.99132
0330f		1766.91224	0.420 671 366	1.683740	3.0154
1110e	(3 1 2)	1880.26574	0.417 464 677	1.748503	0.10750
1110f		1880.26574	0.418 372 995	1.719561	0.21746
0001e	(4 0 1)	2223.75677	0.415 559 510	1.754675	−0.013626
0440e		2356.25242	0.421 218 620	2.720100	171.28

ΔG_v[a]	Type	$v_1v_2l_2v_3$[b]	(P, l_2, i)	G_v	B_v	$D_v \times 10^7$	$H_v \times 10^{12}$	*Observed lines*	n/N[c]	*rms* $\times 10^3$	Notes[d]
Cold bands											
7024.09314(20)	Σ–Σ	3201e – 0000e	(12 0 8)	7024.09314(20)	0.41362720(71)	3.7501(56)	12.55(12)	P62/R60	109/118	0.91	
7024.09258(38)	*Ref. [7]*	*3201e – 0000e*		*7024.09258 (38)*	*0.4136385(19)*	*3.909(23)*	*17.89(73)*		*87/93*	*1.51*	
7029.84337(27)	Σ–Σ	3600e – 0000e	(12 0 9)	7029.84337(27)	0.4198815(29)	12.650(71)	151.2(45)	P33/R32	39/44	0.73	
7037.1740(66)	Δ–Σ	3221e – 0000e	(12 2 15)	7037.1740(66)	0.414503(28)	4.88(38)	136(16)	P67/R58	25/61	0.80	***Perturbed***
7126.97920(12)	Π–Σ	0113e – 0000e	(13 1 1)	7126.97920(12)	0.40893672(21)	1.76492(63)		P63/R53	83/84	0.62	
7126.97881(24)	*Ref. [5]*	*0113e – 0000e*		*7126.97881(24)*	*0.408936885(207)*	*1.76435(154)*					
7126.97901(19)		0113f – 0000e		7126.97901(19)	0.40968970(34)	1.7840(11)		Q61	49/49	0.76	
7126.97880(14)	*Ref. [5]*	*0113f – 0000e*		*7126.97880(14)*	*0.409689927(155)*	*1.786734(911)*					
7137.127161(93)	Σ–Σ	4001e – 0000e	(12 0 10)	7137.127161(93)	0.41096964(21)	2.3416(11)	2.446(15)	P72/R71	130/130	0.47	
7137.12706(29)	*Ref. [5]*	*3201e – 0000e*		*7137.12706(29)*	*0.410968484(319)*	*2.30709(190)*					
7137.12818(21)	*Ref. [7]*	*4001e – 0000e*		*7137.12818(21)*	*0.41096866(91)*	*2.3353(89)*	*2.30(24)*		*98/100*	*0.92*	
7162.65865(49)	Δ–Σ	2421e – 0000e	(12 2 18)	7162.65865(49)	0.41235281(96)	1.2063(47)	−4.363(62)	P70/R70	52/56	0.96	
7179.33012(45)	Π–Σ	0512e – 0000e	(13 1 2)	7179.33012(45)	0.4133916(25)	2.602(23)		P8/R35	13/16	0.71	
7179.33304(74)		0512f – 0000e		7179.33304(74)	0.4154665(28)	2.775(22)		Q35	14/14	1.05	
7194.36540(21)	Σ–Σ	0(12)00e – 0000e	(12 0 11)	7194.36540(21)	0.4176077(18)	8.637(36)	67.9(19)	P34/R36	55/58	0.65	
7214.67949(17)	Σ–Σ	3201e – 0000e	(12 0 12)	7214.67949(17)	0.40961870(53)	0.9689(36)	3.885(57)	P69/R61	85/105	0.78	***Perturbed***
7214.67990(40)	*Ref. [5]*	*4001e – 0000e*		*7214.67990(40)*	*0.409615412(893)*	*0.90342(811)*		*P35/R30*			
7214.68161(32)	*Ref. [7]*	*4001e – 0000e*		*7214.68161(32)*	*0.40961199(98)*	*0.8767(53)*	*−0.01555*		*79/86*	*1.51*	
7325.61159(35)	Π–Σ	0512e – 0000e	(13 1 4)	7325.61159(35)	0.4111037(13)	2.0522(92)		P40/R28	21/27	0.77	
7325.61272(52)		0512f – 0000e		7325.61272(52)	0.4126372(18)	2.130(12)		Q40	21/21	1.23	
7340.79162(13)	Σ–Σ	5200e – 0000e	(12 0 13)	7340.79162(13)	0.41527811(47)	5.3733(39)	25.130(83)	P58/R55	97/99	0.57	
7340.7938(15)	*Ref. [8]*	*5200e – 0000e*		*7340.7938(15)*	*0.4152602(72)*	*5.003(68)*		*P28/R31*	*29/34*	*2.89*	
7355.0324(12)	Δ–Σ	5220e – 0000e	(12 2 23)	7355.0324(12)	0.4157298(25)	−0.642(16)	−24.73(31)	P57/R54	41/47	0.88	
7443.00374(80)	Π–Σ	2112e – 0000e	(13 1 7)	7443.00374(80)	0.409161(39)	5.5(45)	6458(14)	P49/R39	12/38	0.77	***Perturbed***
7463.98521(14)	Σ–Σ	6000e – 0000e	(12 0 14)	7463.98521(14)	0.41279930(35)	3.2658(20)	7.107(29)	P71/R69	126/131	0.72	
7463.98751(41)	*Ref. [7]*	*6000e – 0000e*		*7463.98751(41)*	*0.4127936(16)*	*3.131(12)*	*−0.01555*		*76/85*	*1.86*	
7488.63114(62)	Δ–Σ	5220e – 0000e	(12 2 25)	7488.63114(62)	0.4140493(14)	0.8724(80)	−9.66(14)	P60/R61	60/74	0.90	

7556.13527(11)	Σ–Σ	6000e – 0000e	(12 0 15)	7556.13527(11)	0.41065798(36)	1.6114(27)	7.552(54)	P58/R59	115/115	0.53	
7556.13268(26)	*Ref. [18]*	*6000e – 0000e*		*7556.13268(26)*	*0.4106517(13)*	*1.479(12)*		*P36/R30*		*1.0*	
7556.13769(30)	*Ref. [7]*	*6000e – 0000e*		*7556.13769(30)*	*0.4106569(13)*	*1.600(14)*	*6.76(39)*		*87/93*	*1.27*	
7610.6172(13)	Δ–Σ	3620e – 0000e	(12 2 27)	7610.6172(13)	0.4134127(31)	1.738(21)	– 7.83(44)	P47/R53	22/30	0.83	
7640.47396(14)	Σ–Σ	3600e – 0000e	(12 0 16)	7640.47396(14)	0.41184952(52)	– 0.0812(44)	8.905(99)	P57/R54	97/101	0.60	
7640.47137(41)	*Ref. [18]*	*4400e – 0000e*		*7640.47137(41)*	*0.4118417(22)*	*– 0.261(22)*		*P33/R34*		*1.4*	
7640.45170(16)	*Ref. [6]*	*4400e – 0000e*		*7640.45170(16)*	*0.411845(83)*	*– 0.150(83)*			*35/51*	*3.86*	
7665.27339(10)	Σ–Σ	0203e – 0000e	(14 0 1)	7665.27339(10)	0.40978324(24)	2.5017(13)	3.335(20)	P72/R62	121/123	0.54	
7665.27066(23)	*Ref. [18]*	*0203e – 0000e*		*7665.27066(23)*	*0.40977800(75)*	*2.4183(44)*		*P44/R41*		*1.1*	
7665.27623(40)	*Ref. [7]*	*0203e – 0000e*		*7665.27623(40)*	*0.4097778(14)*	*2.4282(90)*	*– 0.01555*		*81/82*	*1.88*	
7673.63615(81)	Δ–Σ	0223e – 0000e	(14 2 2)	7673.63615(81)	0.4099821(16)	1.1627(84)	– 3.43(13)	P65/R45	42/51	0.78	
Hot bands											
6977.42048(82)	Σ–Σ	0(10)01e – 0200e	(14 0 10)	8145.55278(82)	0.4146299(64)	10.55(12)	203.7(66)	P35/R29	35/47	1.15	**Perturbed**
6977.6654(57)	Δ–Δ	0(10)21e – 0220e	(14 2 20)	8155.4100(57)	0.418916(38)	38.89(62)		P21/R18	10/10	0.71	
6977.6978(71)	Δ–Δ	0(10)21f – 0220f		8155.4425(71)	0.418811(45)	52.50(86)	2062(53)	P29/R27	18/23	0.70	
6991.42204(23)	Σ–Σ	1801e – 1000e	(14 0 12)	8276.32538(23)	0.4115884(13)	3.384(16)	10.31(53)	P44/R45	63/68	0.78	
7000.64433(36)	Π–Π	0911f – 0110f	(13 1 8)	7589.41220(36)	0.4157477(91)	14.64(56)	1091(92)	P59/R59	36/99	0.77	**Perturbed**
7000.64673(27)	Π–Π	0911e – 0110e		7589.41460(27)	0.4131552(33)	6.583(90)	174.9(67)	P60/R53	54/93	0.80	**Perturbed**
7000.6534(12)	*Ref. [8]*	*0911 – 0110*			*0.41427118(67)*	*4.617(76)*	*146(97)*	*P32/R28*	*48/77*	*0.5*	**
7003.52071(47)	Π–Π	4510f – 0110f	(13 1 9)	7592.28858(47)	0.4217215(85)	– 2.72(40)	– 593(52)	P31/R29	26/37	0.61	**Perturbed**
7003.52273(45)	Π–Π	4510e – 0110e		7592.29060(46)	0.4174983(46)	2.170(79)		P24/R23	29/34	1.10	
7037.13535(59)	Π–Σ	0313e – 0200e	(15 1 1)	8205.26765(59)	0.4096133(29)	2.171(25)		P34/R33	23/32	1.20	
7037.13609(60)		0313f – 0200e		8205.26839(60)	0.4110248(30)	2.247(28)		Q33	21/21	1.41	
7076.50686(24)	Σ–Π	0203e – 0110e	(14 0 1)	7665.27473(24)	0.40977454(72)	2.3926(39)		P46/R37	50/56	0.86	
7076.50716((65)		0203e – 0110f		7665.27503(65)	0.4097706(15)	2.3694(58)		Q52	36/36	2.15	
7084.86707(31)	Δ–Π	0223e – 0110e	(14 2 2)	7673.63494(31)	0.40999294(70)	1.2932(26)		P55/R40	50/65	1.20	
7084.86865(50)		0223e – 0110f		7673.63652(50)	0.40998380(85)	1.1805(27)	– 2.98(26)	Q57	43/43	1.53	
7084.86948(23)	Δ–Π	0223f – 0110f		7673.63735(23)	0.40998109(65)	1.8005(35)		P43/R46	50/52	0.81	
7084.86867(40)		0223f – 0110e		7673.63654(40)	0.40998260(80)	1.8028(30)		Q56	38/38	1.35	
7091.44681(14)	Σ–Σ	5001e – 1000e	(14 0 14)	8376.35015(14)	0.40893658(61)	2.1478(59)	5.14(15)	P51/R52	76/79	0.56	
7094.38674(29)	Π–Π	5111f – 0310f	(15 1 12)	8843.45189(29)	0.4132438(13)	2.587(10)		P37/R35	33/39	0.81	
7094.38851(51)	Π–Π	5111e – 0310e		8843.45374(51)	0.4107203(59)	1.41(17)	– 83(13)	P31/R28	22/26	0.77	
7106.18815(68)	Φ–Φ	4331e – 0330e	(15 3 22)	8873.10053(68)	0.4130118(37)	2.006(39)		P31/R22	14/18	0.88	
7106.18979(70)	Φ–Φ	4331f – 0330f		8873.10203(70)	0.4129979(60)	1.73(10)		P23/R22	13/17	0.62	
7108.19349(17)	Σ–Σ	1801e – 0200e	(14 0 12)	8276.32579(17)	0.41158701(95)	3.365(12)	9.82(41)	P45/R44	64/69	0.56	
7116.37553(28)	Δ–Δ	4221e – 0220e	(14 2 22)	8294.12020(28)	0.4123647(12)	0.759(12)	– 8.47(31)	P54/R48	47/57	0.87	
7116.37577(30)	Δ–Δ	4221f – 0220f		8294.12044(30)	0.4123763(13)	2.058(14)	5.37(39)	P49/R49	59/63	0.91	
7126.29615(13)	Π–Π	4111f – 0110f	(13 1 10)	7715.06402(13)	0.41260488(34)	2.0206(21)	1.509(33)	P69/R60	92/98	0.55	
7126.29616(54)		4111f – 0110e		7715.06403(54)	0.4125955(47)	1.909(57)		Q29	16/16	1.33	
7126.29656(12)	Π–Π	4111e – 0110e		7715.06443(12)	0.41075668(27)	1.9404(12)		P64/R44	81/92	0.53	**Perturbed**
7126.29661(93)		4111e – 0110f		7715.06448(93)	0.4107590(50)	1.964(38)		Q36	16/16	2.29	
7126.29780(74)	*Ref. [7]*				*0.4116797(39)*	*1.964(37)*	*– 0.00895*		*80/106*	*3.04*	**
7167.73276(19)	Σ–Σ	3401e – 1000e	(14 0 15)	8452.63610(19)	0.4090365(10)	0.391(13)	6.74(40)	P42/R46	70/72	0.73	
7181.07477(42)	Π–Π	3511e – 1110e	(15 1 16)	9061.34051(42)	0.4086717(24)	1.130(24)		P26/R31	28/33	1.09	
7181.07518(47)	Π–Π	3511f – 1110f		9061.34092(47)	0.4106869(23)	0.662(19)		P36/R32	28/36	1.12	
7208.21777(24)	Σ–Σ	5001e – 0200e	(14 0 14)	8376.35007(24)	0.4089366(14)	2.161(19)	6.56(59)	P42/R46	51/56	0.77	
7229.06470(18)	Π–Π	3311f – 0110f	(13 1 12)	7817.83257(18)	0.41130261(57)	0.9797(40)	2.065(73)	P62/R62	96/100	0.81	
7229.06627(71)		3311f – 0110e		7817.83414(71)	0.4112953(60)	0.924(90)		Q26	17/17	1.65	
7229.06476(19)	Π–Π	3311e – 0110e		7817.83263(19)	0.40971610(56)	1.3332(38)	1.866(68)	P62/R62	98/104	0.80	
7229.06750(90)		3311e – 0110f		7817.83537(90)	0.409666(25)	– 0.5(12)		Q14	12/12	1.57	
7237.06070(25)	Δ–Δ	3421f – 0220f	(14 2 26)	8414.80537(25)	0.4112167(11)	1.225(12)	1.38(35)	P50/R51	64/87	0.76	
7237.06232(28)	Δ–Δ	3421e – 0220e		8414.80699(28)	0.4112147(12)	1.333(12)	– 6.18(31)	P52/R50	63/75	0.87	
7284.50392(24)	Σ–Σ	3401e – 0200e	(14 0 15)	8452.63622(24)	0.4090345(13)	0.364(15)	5.71(43)	P46/R48	53/59	0.82	
7307.59135(48)	Σ–Σ	6200e – 0200e	(14 0 16)	8475.72365(48)	0.4155212(37)	9.326(68)	146.5(32)	P37/R37	33/41	0.96	
7310.11347(41)	Δ–Δ	0(14)20e – 0220e	(14 2 29)	8487.85814(41)	0.4157972(34)	– 3.132(66)	– 78.8(35)	P37/R35	41/49	0.94	
7310.11393(43)	Δ–Δ	0(14)20f – 0220f		8487.85860(43)	0.4158289(58)	3.46(12)		P22/R19	20/25	0.84	
7324.35841(17)	Π–Π	5310f – 0110f	(13 1 13)	7913.12628(17)	0.41719109(30)	3.4107(10)		P59/R59	74/81	0.78	
7324.35927(17)	Π–Π	5310e – 0110e		7913.12714(17)	0.41380885(66)	3.1185(57)	7.06(13)	P56/R58	80/86	0.65	

Table 3 (*continued*)

ΔG_v[a]	Type	$v_1v_2l_2v_3$[b]	(*P*, l_2, *i*)	G_v	B_v	$D_v \times 10^7$	$H_v \times 10^{12}$	*Observed lines*	*n*/*N*[c]	*rms* × 10^3	Notes[d]
7328.04594(35)	Σ–Σ	6200e – 1000e	(14 0 17)	8612.94928(35)	0.4131226(24)	4.884(37)	14.9(15)	P41/R38	36/43	0.71	
7365.81442(31)	Π–Π	0114f – 1110f	(17 1 1)	9246.08016(31)	0.4063063(17)	2.090(18)		P27/R31	29/36	0.79	
7365.81859(41)	Π–Π	0114e – 1110e		9246.08433(41)	0.4055217(26)	1.651(28)		P32/R30	29/38	1.06	
7429.23718(14)	Σ–Σ	0004e – 1000e	(16 0 1)	8714.14052(14)	0.40518430(30)	1.7707(11)		P54/R54	88/95	0.71	
7440.19677(19)	Σ–Σ	7000e – 1000e	(14 0 18)	8725.10011(19)	0.41049903(75)	3.0278(68)	8.92(16)	P52/R55	92/97	0.82	
7444.81607(26)	Σ–Σ	6200e – 0200e	(14 0 17)	8612.94837(26)	0.4131312(14)	5.016(17)	20.34(55)	P48/R47	65/73	0.86	
7453.38658(34)	Δ–Δ	6220e – 0220e	(14 2 31)	8631.13125(34)	0.4138727(26)	– 0.214(49)	– 18.3(24)	P43/R42	43/54	0.85	
7453.38807(34)	Δ–Δ	6220f – 0220f		8631.13274(34)	0.4138718(18)	2.380(23)	3.63(80)	P46/R42	58/66	0.99	
7454.40229(58)	Σ–Σ	0403e – 1000e	(16 0 2)	8739.30563(58)	0.4106898(33)	3.862(38)		P29/R28	19/25	1.01	
7457.58163(17)	Π–Π	6110f – 0110f	(13 1 14)	8046.34950(17)	0.41473933(55)	2.5696(41)	2.578(81)	P61/R58	98/101	0.73	
7457.58225(15)	Π–Π	6110e – 0110e		8046.35012(15)	0.41192897(52)	2.4324(40)	3.542(83)	P61/R55	94/101	0.63	
7522.09958(42)	Φ–Φ	0533e – 0330e	(17 3 3)	9289.01196(42)	0.4114407(27)	1.320(42)	– 16.5(18)	P40/R38	42/45	0.83	
7522.09990(30)	Φ–Φ	0533f – 0330f		9289.01214(30)	0.4114441(11)	1.4601(78)		P40/R34	36/39	0.76	
7525.85900(36)	Σ–Σ	7000e – 1000e	(14 0 19)	8810.76234(36)	0.4095339(39)	1.983(81)	77.2(46)	P43/R41	35/69	1.04	***Perturbed***
7526.07651(59)	Π–Π	0513e – 0310e	(17 1 2)	9275.14174(59)	0.4101376(41)	3.288(71)	51.7(34)	P37/R36	33/39	0.95	
7526.07820(35)	Π–Π	0513f – 0310f		9275.14335(35)	0.41214996(99)	2.7174(53)		P44/R43	38/44	0.91	
7546.00800(18)	Σ–Σ	0004e – 0200e	(16 0 1)	8714.14030(18)	0.40518572(50)	1.7773(25)		P49/R47	71/79	0.82	
7556.96659(36)	Σ–Σ	7000e – 0200e	(14 0 18)	8725.09889(36)	0.4105045(22)	3.115(33)	12.4(13)	P43/R38	48/57	0.97	
7568.84582(22)	Δ–Δ	0423e – 0220e	(16 2 3)	8746.59049(22)	0.41086968(87)	0.0924(80)	– 17.25(20)	P56/R53	65/77	0.79	
7568.84683(21)	Δ–Δ	0423f – 0220f		8746.59150(21)	0.41087207(49)	2.1447(22)		P54/R46	63/71	0.88	
7570.89368(24)	Π–Π	6110f – 0110f	(13 1 5)	8159.66155(24)	0.4130839(33)	2.338(96)	88.7(77)	P45/R44	39/79	0.65	***Perturbed***
7570.89422(49)	Π–Π	6110e – 0110e		8159.66209(49)	0.410679(13)	2.97(93)	195(15)	P56/R51	26/86	0.92	***Perturbed***
7571.17258(20)	Σ–Σ	0403e – 0200e	(16 0 2)	8739.30488(20)	0.41068971(62)	3.9721(43)	16.208(79)	P57/R62	77/88	0.80	
7582.34957(28)	Δ–Δ	5420f – 022f	(14 2 33)	8760.09424(28)	0.41256756(90)	1.4906(52)		P43/R41	46/54	0.90	
7582.34981(31)	Δ–Δ	5420e – 0220e		8760.09448(31)	0.4125680(12)	0.9840(65)		P42/R41	38/45	0.96	
7592.13624(52)	Σ–Σ	1203e – 1000e	(16 0 4)	8877.03958(52)	0.4079962(42)	2.975(80)	31.3(39)	P37/R36	36/43	1.09	
7616.50013(14)	Π–Π	0313f – 0110f	(15 1 1)	8205.26800(14)	0.41102312(18)	2.19626(43)		P72/R66	99/105	0.75	
7616.50069(61)		0313f – 0110e		8205.26856(61)	0.4110248(34)	2.224(34)		Q32	25/25	1.53	
7616.50075(14)	Π–Π	0313e – 0110e		8205.26862(14)	0.40960304(38)	2.0926(23)	0.989(37)	P69/R58	94/109	0.63	
7616.50041(93)		0313e – 0110f		8205.26828(93)	0.4096011(70)	2.036(85)		Q29	19/19	2.10	
7616.48787(74)	*Ref. [18]*				*0.4103094(40)*	*2.085(42)*		*P23/R30*		*2.5*	**
7637.13737(97)	Γ–Γ	1443e – 0440e	(18 4 12)	9993.38979(97)	0.409819(10)	3.03(31)	254(26)	P28/R21	21/23	0.82	
7656.9883(12)	Π–Π	2113e – 1110e	(17 1 7)	9537.2540(12)	0.4056527(88)	2.55(12)		P0/R25	8/8	0.67	
7657.00199(56)	Π–Π	2113f – 1110f		9537.26773(56)	0.4065991(40)	1.334(55)		P0/R27	13/13	0.74	
7664.7999(59)	Σ–Σ	1004e – 0001e	(18 0 4)	9888.5567(59)	0.403379(22)	2.05(19)		P0/R29	8/8	0.85	
7674.09772(25)	Φ–Φ	1333e – 0330e	(17 3 7)	9441.01010(25)	0.40909316(60)	1.5825(27)		P50/R36	52/56	0.82	
7677.51571(22)	Π–Π	3710f – 0110f	(13 1 16)	8266.28358(22)	0.41338838(86)	0.4001(83)	3.75(21)	P54/R44	65/71	0.69	
7677.51606(23)	Π–Π	3710e – 0110e		8266.28393(23)	0.4108023(10)	0.974(10)	4.95(29)	P52/R40	54/60	0.69	
7691.58471(22)	Σ–Σ	2003e – 1000e	(16 0 7)	8976.48805(22)	0.4051391(12)	1.763(13)	5.76(37)	P59/R51	54/90	0.79	***Perturbed***
7708.90887(15)	Σ–Σ	1203e – 0200e	(16 0 4)	8877.04117(15)	0.40796951(50)	2.4140(37)	2.901(71)	P62/R56	88/91	0.68	
7710.77493(26)	Δ–Δ	1223e – 0220e	(16 2 7)	8888.51960(26)	0.4083782(26)	1.395(61)	20.3(38)	P58/R55	41/82	0.65	***Perturbed***
7710.77509(21)	Δ–Δ	1223f – 0220f		8888.51975(22)	0.40837396(97)	1.8050(77)	2.64(17)	P57/R51	54/90	0.74	***Perturbed***
7710.7630(23)	Ref. [8]	1223 – 0220			0.408451(15)	1.15(19)		P19/R26	22/33	0.74	**
7747.02908(18)	Π–Π	1113e – 0110e	(15 1 3)	8335.79695(18)	0.40719639(22)	1.70677(53)		P67/R67	76/99	0.63	
7747.02942(22)	Π–Π	1113f – 0110f		8335.79729(22)	0.40803813(24)	1.67948(55)		P70/R67	79/100	0.81	
7747.01366(72)	*Ref. [18]*	1113 – 0110			*0.4076223(33)*	*1.738(27)*		*P37/R35*		*4.2*	**
7747.03196(61)	Ref. [7]	1113 – 0110			0.4076168(21)	1.700(13)			104/133	3.35	**

Notes: the uncertainties are given in parenthesis in the unit of the last quoted digit. When a given band has been previously analyzed, the corresponding spectroscopic parameters are given in italics for comparison. In several cases indicated by ** in the last column the comparison is not straightforward because a different expression was used for the energy levels leading to a different definition of the parameters

[a] Difference between the upper and lower vibrational term values.

[b] Normal mode labeling according to the maximum value of the modulo of the expansion coefficients of an eigenfunction.

[c] *n*: number of transitions included in the fit; *N*: number of assigned rotational transitions.

[d] Notes indicating the bands affected by rovibrational perturbations (see Table 5) and when a different expression was used for the energy levels (**).

Table 4
Spectroscopic parameters (in cm^{-1}) of the rovibrational bands of $^{14}N^{15}N^{16}O$, $^{15}N^{14}N^{16}O$ and $^{14}N_2{}^{18}O$ recorded by CW-CRDS between 6950 and 7653 cm^{-1}.

Lower state constants [5]

Isotope	State $v_1v_2l_2v_3$	(P, l_2, i)	G_v	B_v	$D_v \times 10^7$
$^{14}N^{15}N^{16}O$	0000e	(001)	0.0	0.418 981 810	1.763264
	0110e	(111)	575.43365	0.419 108 916	1.785826
	0110f		575.43365	0.419 918 641	1.794459
$^{15}N^{14}N^{16}O$	0000e	(001)	0.0	0.404 857 965	1.642938
	0110e	(111)	585.31212	0.405 037 265	1.656798
	0110f		585.31212	0.405 781 109	1.667421
$^{14}N_2{}^{18}O$	0000e	(001)	0.0	0.395 577 895	1.583456

ΔG_v[a]	Type	$v_1v_2l_2v_3$[b]	(P, l_2, i)	G_v	B_v	$D_v \times 10^7$	$H_v \times 10^{12}$	*Observed lines*	*n/N*[c]	*rms* × 10^3
$^{14}N^{15}N^{16}O$										
7051.77618(22)	Σ–Σ	2401e – 0000e	(12 0 10)	7051.77618(22)	0.41113485(64)	2.4414(30)		P50/R48	52/67	0.89
7051.77452(94)	*Ref. [19]*	*2401e – 0000e*		*7051.77452(94)*	*0.41114508(47)*	*2.5633(55)*	*3.71(17)*	*P49/R47*	*92/95*	*0.39*
7143.39642(22)	Σ–Σ	4001e – 0000e	(12 0 12)	7143.39642(22)	0.40850484(52)	1.4314(23)		P47/R50	58/70	0.74
7143.39539(15)	*Ref. [19]*	*4001e – 0000e*		*7143.39539(15)*	*0.40850952(63)*	*1.4844(62)*	*1.52(16)*	*P53/R50*	*100/103*	*0.64*
7149.73186(49)	Π–Π	4111e – 0110e	(13 1 12)	7725.16551(49)	0.4087781(17)	1.531(12)		P32/R38	21/23	1.02
7149.73271(40)	*Ref. [19]*			*7725.16636(40)*	*0.4087723(27)*	*1.449(42)*	*−2.7(18)*	*P35/R40*	*55/64*	*1.23*
7149.73029(51)	Π–Π	4111f – 0110f		7725.16394(51)	0.4100903(18)	1.360(11)		P26/R38	17/21	0.85
7149.72916(44)	*Ref. [19]*			*7725.16281(44)*	*0.4100978(49)*	*1.54(13)*	*8.0(89)*	*P31/R30*	*45/50*	*1.09*
7384.08114(44)	Σ–Σ	5200e – 0000e	(12 0 14)	7384.08114(44)	0.4129669(17)	3.928(12)		P37/R37	29/30	1.03
7492.12225(23)	Σ–Σ	6000e – 0000e	(12 0 15)	7492.12225(23)	0.41043532(69)	2.3478(38)		P42/R46	57/63	0.94
7492.12183(24)	*Ref. [19]*	*6000e – 0000e*		*7492.12183(24)*	*0.4104420(13)*	*2.443(15)*	*3.31(51)*	*P43/R46*	*85/89*	*0.95*
7511.63742(27)	Σ–Σ	0203e – 0000e	(14 0 1)	7511.63742(27)	0.41012966(97)	2.6862(59)		P42/R41	52/56	0.98
7511.63778(32)	*Ref. [19]*	*0203e – 0000e*		*7511.63778(32)*	*0.4101315(17)*	*2.669(21)*	*−2.95(67)*	*P39/R47*	*76/87*	*1.27*
7567.42857(25)	Σ–Σ	5200e – 0000e	(12 0 16)	7567.42857(25)	0.40922203(96)	0.6763(67)		P40/R35	37/40	0.77
7567.42959(33)	*Ref. [19]*	*5200e – 0000e*		*7567.42959(33)*	*0.4092254(24)*	*0.778(41)*	*5.6(19)*	*P40/R37*	*73/77*	*1.14*
7614.99821(30)	Π–Π	1113e – 0110e	(15 1 3)	8190.43186(30)	0.40740025(71)	1.7414(29)		P52/R45	48/61	1.03
7614.99969(37)	*Ref. [19]*	*1113e – 0110e*		*8190.43334(37)*	*0.4073935(23)*	*1.633(35)*	*−5.0(15)*	*P41/R40*	*65/76*	*1.05*
7614.99918(36)	Π–Π	1113f – 0110f		8190.43283(36)	0.40822539(93)	1.7267(49)		P47/R49	44/62	0.95
7614.99970(44)	*Ref. [19]*	*1113f – 0110f*		*8190.43335(44)*	*0.4082234(17)*	*1.690(17)*	*−1.40(45)*	*P49/R50*	*78/94*	*1.36*
7650.75391(14)	Σ–Σ	1003e – 0000e	(14 0 3)	7650.75391(14)	0.40710144(29)	1.7305(11)		P58/R54	87/93	0.71
7650.754129(91)	*Ref. [19]*	*1003e – 0000e*		*7650.754129(91)*	*0.40710222(34)*	*1.7366(28)*	*0.125(62)*	*P59/R55*	*110/115*	*0.43*
$^{15}N^{14}N^{16}O$										
6957.90001(24)	Σ–Σ	3201e – 0000e	(12 0 8)	6957.90001(24)	0.3996417(12)	3.030(13)	5.31(38)	P43/R49	70/78	0.96
6957.90065(20)	*Ref. [23]*	*3201e – 0000e*		*6957.90065(20)*	*0.3996444(11)*	*3.079(13)*	*7.31(43)*	*P45/R47*	*80/93*	*0.76*
7065.52503(16)	Σ–Σ	4001e – 0000e	(12 0 10)	7065.52503(16)	0.39714465(70)	2.0787(70)	2.24(18)	P53/R52	82/89	0.63
7065.52508(11)	*Ref. [23]*	*4001e – 0000e*		*7065.52508(11)*	*0.39714574(49)*	*2.0935(49)*	*2.79(13)*	*P53/R52*	*97/106*	*0.49*
7142.12900(29)	Σ–Σ	3201e – 0000e	(12 0 12)	7142.12900(29)	0.3965357(24)	0.809(49)	11.8(27)	P54/R48	47/68	0.67
7142.12893(10)	*Ref. [23]*	*3201e – 0000e*		*7142.12893(10)*	*0.39653682(83)*	*0.817(16)*	*12.60(86)*	*P48/R46*	*71/92*	*0.34*
7275.89959(42)	Σ–Σ	5200e – 0000e	(12 0 13)	7275.89959(42)	0.4013031(20)	4.092(17)		P30/R33	28/35	0.99
7394.27126(21)	Σ–Σ	6000e – 0000e	(12 0 14)	7394.27126(21)	0.3988730(11)	2.771(12)	5.19(34)	P50/R47	63/74	0.75
7394.27264(31)	*Ref. [23]*	*6000e – 0000e*		*7394.27264(31)*	*0.3988685(11)*	*2.6692(71)*		*P35/R42*	*57/76*	*1.15*
7482.85586(23)	Σ–Σ	6000e – 0000e	(12 0 15)	7482.85586(23)	0.3974422(11)	0.9332(91)		P35/R38	53/57	0.82

Table 4 (*continued*)

ΔG_v[a]	Type	$v_1v_2l_2v_3$[b]	(P, l_2, i)	G_v	B_v	$D_v \times 10^7$	$H_v \times 10^{12}$	*Observed lines*	n/N[c]	*rms* $\times 10^3$
7482.85694(31)	*Ref. [23]*	*6000e – 0000e*		*7482.85694(31)*	*0.3974403(11)*	*0.8931(64)*		*P38/R42*	*62/80*	*1.31*
7543.01230(88)	Π–Π	0313e – 0110e	(15 1 1)	8128.32442(88)	0.3956663(34)	1.809(25)		P35/R34	13/20	0.95
7592.48593(22)	Σ–Σ	0203e – 0000e	(14 0 1)	7592.48593(22)	0.39584103(92)	2.2206(95)	1.86(26)	P59/R56	71/89	0.75
7592.48600(36)	*Ref. [23]*	*0203e – 0000e*		*7592.48600(36)*	*0.3958415(12)*	*2.1972(77)*		*P48/R45*	*69/92*	*1.55*
7667.80351(47)	Π–Π	1113f – 0110f	(15 1 3)	8253.11563(47)	0.3943280(19)	1.961(16)		P36/R24	29/38	1.04
7667.8096(18)	*Ref. [23]*	*1113f – 0110f*		*8253.1217(18)*	*0.3942929(81)*	*1.548(78)*		*P37/R37*	*16/69*	*1.38*
7667.80615(63)	Π–Π	1113e – 0110e		8253.11827(63)	0.3934954(17)	1.5829(91)		P44/R23	30/44	1.13
7667.8111(22)	*Ref. [23]*	*1113e – 0110e*		*8253.1232(22)*	*0.3943851(14)*	*1.535(32)*		*P37/R37*	*15/71*	*1.36*
7702.49962(11)	Σ–Σ	1003e – 0000e	(14 0 3)	7702.49962(11)	0.39310710(21)	1.57079(68)		P62/R54	89/90	0.60
7702.50017(18)	*Ref. [23]*	*1003e – 0000e*		*7702.50017(18)*	*0.39310735(42)*	*1.5688(17)*		*P55/R53*	*88/105*	*0.93*
$^{14}N_2{}^{18}O$										
7006.34090(21)	Σ–Σ	4001e – 0000e	(12 0 10)	7006.34090(21)	0.38782404(63)	1.5451(34)		P47/R45	56/59	0.85
7292.37472(18)	Σ–Σ	6000e – 0000e	(12 0 14)	7292.37472(18)	0.38919506(70)	2.0837(48)		P40/R38	54/55	0.67
7376.57168(28)	Σ–Σ	6000e – 0000e	(12 0 15)	7376.57168(28)	0.3893843(12)	0.1301(84)		P30/R37	46/49	0.94
7630.84253(23)	Σ–Σ	0203e – 0000e	(14 0 1)	7630.84253(23)	0.38684063(75)	2.1581(47)		P44/R40	47/53	0.83
7718.94790(15)	Σ–Σ	1003e – 0000e	(14 0 3)	7718.94790(15)	0.38433900(28)	1.43632(99)		P57/R54	89/92	0.71

Notes: the uncertainties are given in parenthesis in the unit of the last quoted digit.
[a] Difference between the upper and lower vibrational term values.
[b] Normal mode labeling according to the maximum value of the modulo of the expansion coefficients of an eigenfunction.
[c] *n*: number of transitions included in the fit; *N*: number of assigned rotational transitions.

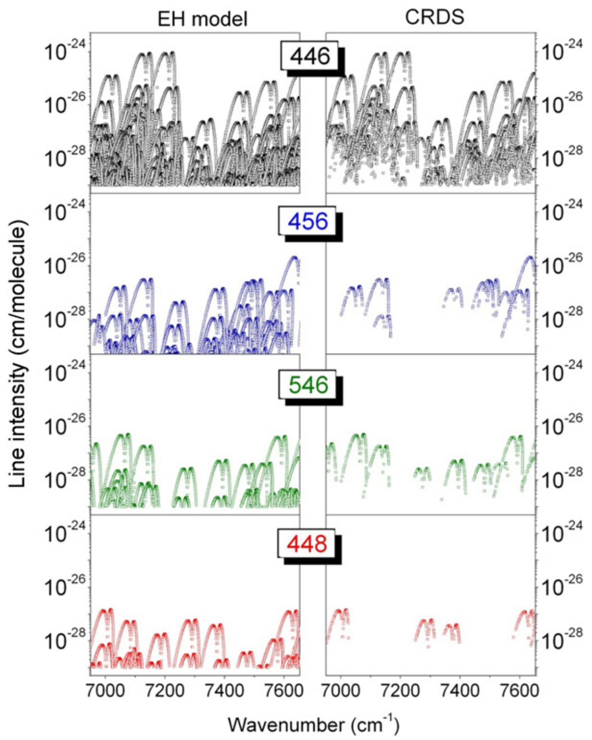

Fig. 4. Overview comparison of the absorption spectrum of $^{14}N_2{}^{16}O$, $^{15}N^{14}N^{16}O$, $^{14}N^{15}N^{16}O$ and $^{14}N_2{}^{18}O$ in normal isotopic abundance between 6950 and 7653 cm^{-1}. The line intensities are estimated values which were calculated using the set of $^{14}N_2{}^{16}O$ effective dipole moment parameters of Ref. [17]. *Right hand*: CRDS line list; *Left hand*: spectra predicted by the effective Hamiltonian and dipole moment models.

for a better determination of the spectroscopic constants, in particular the distortion constants.

Among the 71 bands analyzed, 51 are hot bands. As an illustration of the sensitivity of the recordings, let us note that the highest excited vibrational state observed in this study is the (14^43) state at 9993.4 cm^{-1} which belongs to the $P=18$ polyad. It was observed through the (14^43)–(04^40) hot band ($\Delta P=14$) at 7657 cm^{-1} while the relative population of the (04^40) lower state is only 1.06×10^{-5} at room temperature.

A number of newly observed bands reach upper states which were previously accessed through different bands in other spectral regions, in particular, those reported as upper states of cold bands measured by ICLAS-VeCSEL in the 8800–10,000 cm^{-1} region [20–22]. The present CRDS measurements decrease by about a factor of five the uncertainty on the upper energy levels previously measured by ICLAS-VeCSEL.

3.2.2. $^{14}N^{15}N^{16}O$ and $^{15}N^{14}N^{16}O$

The assignment of the $^{14}N^{15}N^{16}O$ and $^{15}N^{14}N^{16}O$ transitions benefited from the quality of the EH predictions relying on extensive measurements performed from FTS spectra recorded with a high isotopic enrichment (>97%) and absorption pathlength up to 105 m [19,23]. Nine and ten bands were assigned for the $^{14}N^{15}N^{16}O$ and $^{15}N^{14}N^{16}O$ species in normal isotopic abundance (0.0036409 [15]) in

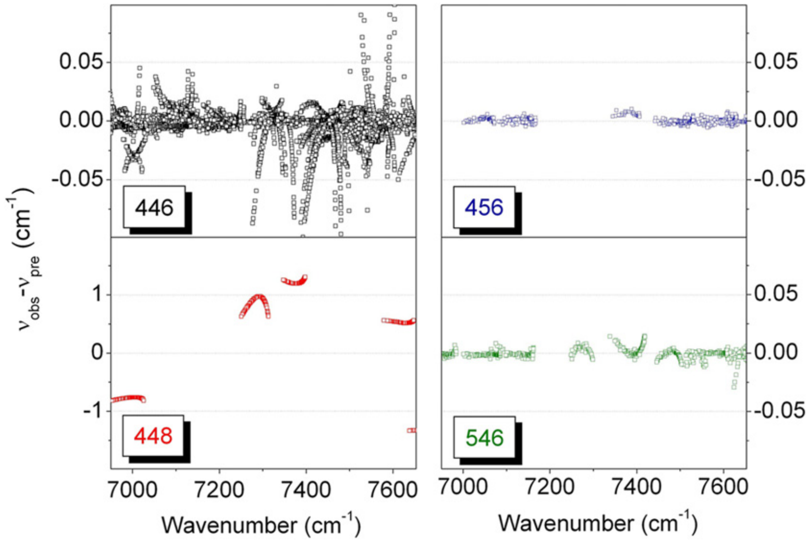

Fig. 5. Differences between the line positions of the $^{14}N_2{}^{16}O$, $^{15}N^{14}N^{16}O$, $^{14}N^{15}N^{16}O$ and $^{14}N_2{}^{18}O$ isotopologues of nitrous oxide assigned in the CW-CRDS spectrum between 6950 and 7653 cm^{-1} and their values predicted by the corresponding effective rovibrational Hamiltonians [9–11].

Table 5
Observed perturbations of the $^{14}N_2{}^{16}O$ bands between 6950 and 7653 cm^{-1}.

Band affected	Center (cm^{-1})	Upper vibrational state	Perturber	J_{pert}[a]	Interaction type[b]
3221–0000	7037.17	(12 2 15)	(12 2 16)	Smooth	Anharmonic
3201–0000	7214.68	(12 0 12)	(12 2 20)	34	Anharmonic + ℓ-type
			(12 0 11)	57	Anharmonic
2112–0000	7443.00	(13 1 7)	(13 1 6)	17	Anharmonic [3]
0(10)01–0200[c]	6977.42	(14 0 10)	(14 0 11)	Smooth	Anharmonic [3]
0911–0110	7000.64	(13 1 8)	(13 1 9)	Smooth	Anharmonic [3]
4510–0110	7003.52	(13 1 9)	(13 1 8)	Smooth	Anharmonic [3]
4111e–0110e	7126.30	(13 1 10)	(14 0 2)	Smooth	Interpolyad coriolis
6200–1000	7525.86	(14 0 19)	(16 0 3)	24	Interpolyad anharmonic
6110–0110	7570.89	(13 1 15)	(14 2 20)	*e*: 17	Interpolyad coriolis
			(14 2 19)	*e*: 27, *f*: 21	Interpolyad coriolis
2003–1000	7691.58	(16 0 7)	(16 0 6)	32	Anharmonic [4,21]
1223–0220	7710.77	(16 2 7)	(15 1 13)	*e* and *f*: 32	Interpolyad coriolis [4]

[a] Value of the angular momentum quantum number at which the energy level crossing takes place.
[b] When the perturbation of the upper level has been analyzed through a different band, the corresponding reference is given.
[c] For clarity, ν_2 values larger than 9 are written between parenthesis.

our sample, respectively. For both isotopologues, one band not reported from the FTS spectra of the pure species could be identified.

The retrieved spectroscopic parameters of the $^{14}N^{15}N^{16}O$ and $^{15}N^{14}N^{16}O$ bands are listed in Table 4. The comparison with the FTS results [19,23] included in this Table shows an excellent agreement.

3.2.3. $^{14}N_2{}^{18}O$

To the best of our knowledge, there are no spectroscopic studies of $^{14}N_2{}^{18}O$ with a high isotopic enrichment in our spectral region. Among the five bands analyzed (Table 4) three are newly reported while two near the borders of the investigated region were already included in our previous studies [3,4].

4. Discussion

4.1. Comparison with the effective Hamiltonian predictions

An overview comparison of the CRDS observations with the predictions of the effective operator models is presented in Fig. 4. The line intensities used for this plot are estimated values which were calculated using the set of $^{14}N_2{}^{16}O$ effective dipole moment parameters of Ref. [17]. The weakest lines have intensity in the order of 10^{-29} cm/molecule, about four orders of magnitude smaller than the weakest N_2O line included in the HITRAN line list. The differences between the measured line positions and their predicted values [9–11] are displayed in Fig. 5 for the four isotopologues.

As a result of the very recent fit of the EH parameters to the line positions collected from an exhaustive review

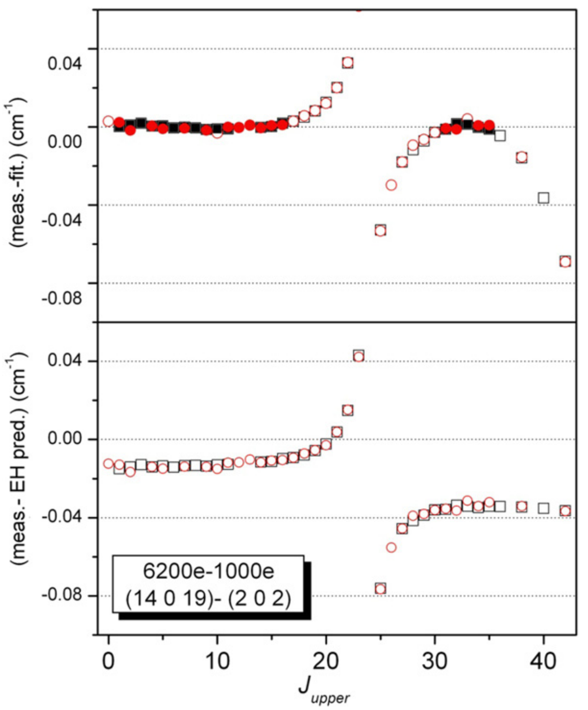

Fig. 6. Differences between the measured values of the transition wavenumbers of the 6200–1000 band at 7525.86 cm^{-1} and the corresponding values calculated using the spectroscopic parameters of Table 3 (*upper panel*) and the EH model (*lower panel*). For each J_{upper} value, the values corresponding to the $R(J_{upper}-1)$ (square) and $P(J_{upper}+1)$ (circles) transitions are plotted. The solid symbols in the upper panels indicate the transitions used as input data in the fit of the spectroscopic parameters. The (14 0 19) upper state is perturbed by an *interpolyad* anharmonic interaction with the (16 0 3) state.

of the literature [9], the predictive capabilities of the EH model of the main isotopologue is found to be very good. This new global modeling of $^{14}N_2{}^{16}O$ line positions has allowed reproducing 37,353 line positions of 325 bands measured in the 0–9700 cm^{-1} region, with a root mean square deviation of 0.00423 cm^{-1} [9]. As Fig. 5 shows, the average (obs. − calc.) deviation is −0.0021(141) cm^{-1} which is consistent with the *rms* deviation of the global fit. Nevertheless some residuals reach values as high as 0.1 cm^{-1}, in particular for the high *J* levels of the 6110–0110 and 5200–0000 bands. The newly measured line positions will therefore help to further improve the set of effective Hamiltonian parameters of the main isotopologue.

The transitions of $^{14}N^{15}N^{16}O$ and $^{15}N^{14}N^{16}O$ observed in "natural" abundance in the present CRDS spectra are expected to be well reproduced by the recent EH models developed by Tashkun et al. [10] because these fits benefited from numerous FTS observations obtained with pure isotopic samples. Indeed, most of the transitions presently identified were previously measured by FTS [19,23] and included as input data. In consequence, the deviations are limited ($+0.23(248)\times10^{-3}$ and $-0.49(377)\times10^{-3}$ cm^{-1} on average for $^{14}N^{15}N^{16}O$ and $^{15}N^{14}N^{16}O$, respectively), the largest deviations being about 0.02 cm^{-1} for high *J* transitions of the 6000–0000 band of $^{15}N^{14}N^{16}O$.

Due to a lack of experimental information, larger deviations are observed for the $^{14}N_2{}^{18}O$ species because many important parameters are absent in the preliminary effective Hamiltonian developed for this isotopologue [11]. As a result, for the five bands analyzed, the deviations of the measured positions from their predicted values range between −1.5 and 1.5 cm^{-1} (Fig. 5).

4.2. Rovibrational perturbations

Eleven bands of $^{14}N_2{}^{16}O$ were found to be clearly affected by perturbations which obliged us to exclude a significant number of line positions from the input data used to derive the spectroscopic parameters (see Table 3). The perturbation shows up as a local or smooth perturbation depending on the existence of an energy crossing in the range of observations. When the perturbation is due to a coupling between vibrational states belonging to the same polyad, it is generally satisfactorily reproduced by the EH model but in the case of *interpolyad* interactions (Coriolis or anharmonic), the line positions calculated from the effective Hamiltonian or from the spectroscopic parameters (Table 3) deviate in a similar way from the measured values. The perturber and interaction mechanism of an interpolyad coupling can nevertheless be identified from the energy crossings predicted by the effective Hamiltonian model. The *J* values corresponding to the energy crossing of the interacting states and the coupling mechanism are listed in Table 5 for each of the eleven perturbed bands. Some of the observed perturbations were analyzed in our previous works through bands reaching the same (perturbed) upper state from different lower states (the corresponding reference is indicated in the last column of the table). As an example of interpolyad anharmonic interaction, Fig. 6 shows a reduced energy plot for the 6200–1000 band at 7525.86 cm^{-1}. The (14 0 19) upper state is perturbed by the (16 0 3) state with an energy crossing around $J=24$, well predicted by the EH model. As expected in the case of an interpolyad coupling, the effect of the perturbation is also clearly apparent on the differences between the measurements and the EH predictions (Fig. 6). This is also the case for the perturbations affecting the (13 1 15) state (Fig. 7) coupled to the (14 2 19) and (14 2 20) states by interpolyad Coriolis interactions. On the contrary, the two intrapolyad interactions (anharmonic + *l*-type and anharmonic) affecting the (12 0 12) upper state of the 3201–0000 band are satisfactorily reproduced by the EH model (Fig. 7).

5. Conclusion

This contribution completes our CRDS investigations of nitrous oxide [1–4] in the spectral range accessible with our set of seventy DFB laser diodes. In the presently investigated region (6950–7653 cm^{-1}) more than 7200 transitions were measured and rovibrationally assigned to four N_2O isotopologues. It leads to an overall number of about 20,000 transitions for the entire 5900–7920 cm^{-1} range. The assignment procedure based on the predictions of the EH models was a very laborious

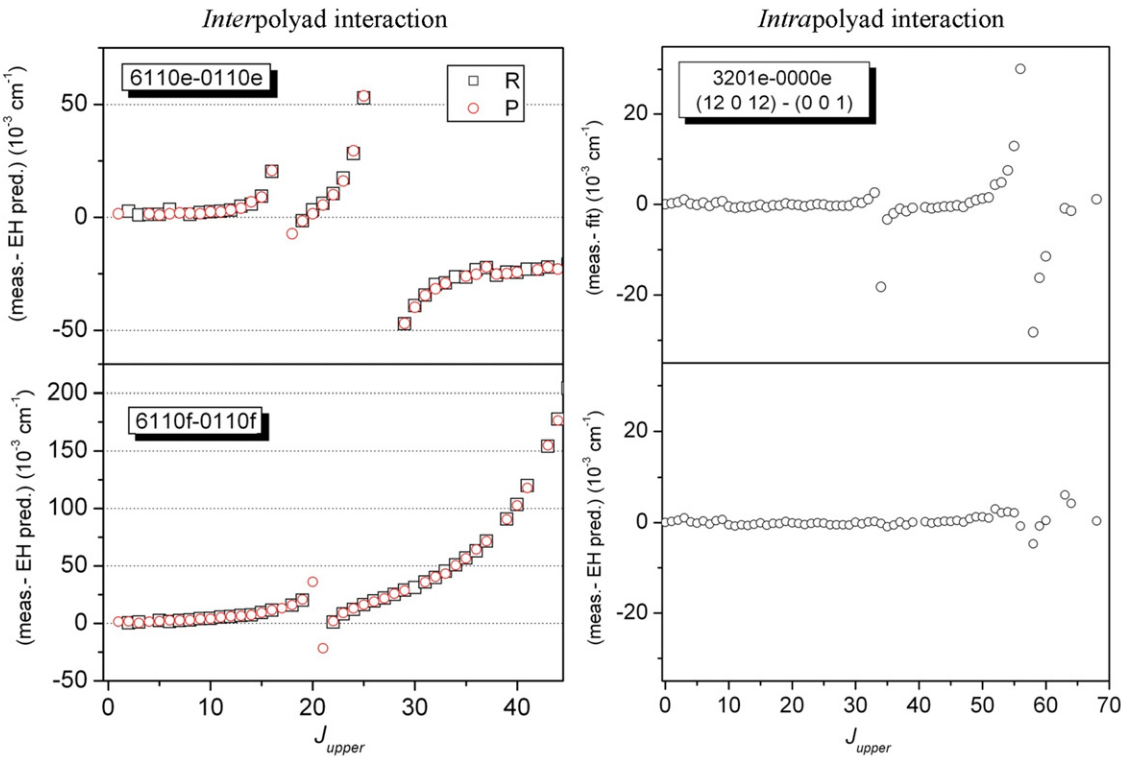

Fig. 7. *Left hand*: differences between the measured values of the transition wavenumbers of the 6110–0110 band at 7570.89 cm^{-1} and the corresponding values calculated using the EH model for the *e* (*upper panel*) and *f* (*lower panel*) sublevels. For each J_{upper} value, the values corresponding to the $R(J_{upper}-1)$ (square) and $P(J_{upper}+1)$ (circles) transitions are plotted. The (13 1 15) upper state is perturbed by interpolyad Coriolis interactions with the (14 2 19) and (14 2 20) states. *Right hand*: differences between the measured values of the *P*(*J*) transition wavenumbers of the 3201–0000 band at 7214.68 cm^{-1} and the corresponding values calculated using the spectroscopic parameters of Table 3 (*upper panel*) and the EH model (*lower panel*). The (12 0 12) upper state is affected by two intrapolyad interactions: (anharmonic + *l*-type) with (12 2 20) and anharmonic with (12 0 11).

task as a result of the high density of observed transitions (more than 10 lines/cm^{-1}) and of the contribution of the five most abundant N_2O isotopologues. Most of the measured transitions belong to weak hot bands of $^{14}N_2{}^{16}O$. Consequently the derived information concerns many levels with a high vibrational excitation up to 10,000 cm^{-1}, much above the high energy limit of the CRDS recordings. The set of our previous CRDS measurements [1–4] was a major source of the input data used in the recent new fit of the parameters of global effective Hamiltonian model of $^{14}N_2{}^{16}O$ [9]. From an exhaustive review of the literature, 37,533 measured line positions were collected in the 0–9700 cm^{-1} region and reproduced with a root mean square deviation of 0.00423 cm^{-1}. Nevertheless, more work is still needed to improve the modeling and approach the experimental accuracy (0.001 cm^{-1} for the CRDS measurements): the developed model is a polyad modeling which cannot reproduce the observations in the case of interpolyad couplings (see above). This is why only $P \leq 17$ bands were considered and about 2% of the observed line positions had to be excluded from the input data of the fit of the EH parameters [9]. The development of a non-polyad effective Hamiltonian which is in progress at IAO Tomsk, should help to decrease the (obs. − calc.) *rms* deviation and assign part of the lines left unassigned in our CRDS spectra. Indeed, all over the CRDS recordings a significant fraction of lines (10–20%) remained unassigned. We believe that most of them are due to N_2O isotopologues. Our assignment procedure relying mostly on the EH predictions, the failure to assign these lines may indicate that some important improvements are still needed in the modeling. Line intensities may provide valuable insights for the assignment of the remaining lines which are all weak or very weak. Nevertheless, the present status of the line intensity modeling based on the measurements of Ref. [17] is not fully satisfactory when extrapolated to the weak bands unobserved in Ref. [17], because some important dipole moment parameters are unknown. For instance, some bands predicted with intensity largely above the CRDS sensitivity threshold were not detected, indicating that the corresponding predicted intensities are overestimated. As a continuation of the present work, in a future contribution, we will present the intensity retrieval of a selected set of bands which will allow to improve the set of effective dipole parameters of the $\Delta P = 12$–14 bands.

Acknowledgments

This work is jointly supported by CNRS (France), CAS (China) and RFBR (Russia) in the frame of Groupement de Recherche International SAMIA (Spectroscopie d'Absorption des Molécules d'Intérêt Atmosphérique), as well as by RFBR-CNRS (N 09-05-93105), RFBR-NSFC (10-05-91176), NSFC (20903085, 20873132) and NKBRSF (2010CB92330).

Appendix A. Supplementary materials

Supplementary data associated with this article can be found in the online version at doi:10.1016/j.jqsrt.2012.03.005.

References

[1] Liu AW, Kassi S, Malara P, Romanini D, Perevalov VI, Tashkun SA, et al. High sensitivity CW-cavity ring down spectroscopy of N_2O near 1.5 l μm (I). J Mol Spectrosc 2007;244:33–47.
[2] Liu AW, Kassi S, Perevalov VI, Tashkun SA, Campargue A. High sensitivity CW-cavity ring down spectroscopy of N_2O near 1.5 l μm (II). J Mol Spectrosc 2007;244:48–62.
[3] Liu AW, Kassi S, Perevalov VI, Hu SM, Campargue A. High sensitivity CW-cavity ring down spectroscopy of N_2O near 1.5 μm (III). J Mol Spectrosc 2009;254:20–7.
[4] Liu AW, Kassi S, Perevalov VI, Tashkun SA, Campargue A. High sensitivity CW-Cavity Ring Down Spectroscopy of N_2O near 1.28 μm. J Mol Spectrosc 2011;267:191–9.
[5] Toth RA. Line positions and strengths of N_2O between 3515 and 7800 cm − 1. J Mol Spectrosc 1999;197:158–87.
[6] Campargue A, Permogorov D, Bach M, Abbouti Temsamani M, Vander Auwera J, Fujii M. Overtone spectroscopy in nitrous oxide. J Chem Phys 1995;103:5931–8.
[7] Weirauch G, Kachanov AA, Campargue A, Bach M, Herman M, Vander Auwera J. Refined investigation of the overtone spectrum of nitrous oxide. J Mol Spectrosc 2000;202:98–106.
[8] Wang L, Perevalov VI, Tashkun SA, Gao B, Hao LY, Hu SM. Fourier transform spectroscopy of N_2O weak overtone transitions in the 1–2 μm region. J Mol Spectrosc 2006;237:129–36.
[9] Perevalov VI, Tashkun SA, Kochanov RV, Liu AW, Campargue A. Global modeling of the line positions of $^{14}N_2{}^{16}O$ within the framework of the polyad model of effective Hamiltonian. JQSRT 2012. doi:10.1016/j.jqsrt.2011.12.008.
[10] Tashkun SA, Perevalov VI, Kochanov RV, Liu AW, Hu SM. Global fittings of $^{14}N^{15}N^{16}O$ and $^{15}N^{14}N^{16}O$ vibrational–rotational line positions using the effective Hamiltonian approach. JQSRT 2010;111:1089–105.
[11] Vlasova AV, Perevalov BV, Tashkun SA, Perevalov VI. Global fittings of the line positions of the rare isotopic species of the nitrous oxide molecule. In: Proceedings of the XVth symposium on high-resolution molecular spectroscopy, vol. 6580. Nizhny Novgorod, Russia: SPIE; 2006. p. 658007.
[12] Macko P, Romanini D, Mikhailenko SN, Naumenko OV, Kassi S, Jenouvrier A, et al. High sensitivity CW-cavity ring down spectroscopy of water in the region of the 1.5 m atmospheric window. J Mol Spectrosc 2004;227:90–108.
[13] Morville J, Romanini D, Kachanov AA, Chenevier M. Two schemes for trace detection using cavity ringdown spectroscopy. Appl Phys 2004;D78:465–76.
[14] Perevalov BV, Kassi S, Romanini D, Perevalov VI, Tashkun SA, Campargue A. CW-cavity ringdown spectroscopy of carbon dioxide isotopologues near 1.5 μm. J Mol Spectrosc 2006;238:241–55.
[15] Rothman LS, Gordon IE, Barbe A, Benner DC, Bernath PF, Birk M, et al. The HITRAN 2008 molecular spectroscopic database. JQSRT 2009;110:533–72.
[16] Teffo JL, Perevalov VI, Lyulin OM. Reduced effective Hamiltonian for global treatment of rovibrational energy levels of nitrous oxide. J Mol Spectrosc 1994;168:390–403.
[17] Daumont L, Vander Auwera J, Teffo JL, Perevalov VI, Tashkun SA. Line intensity measurements in $^{14}N_2{}^{16}O$ and their treatment using the effective dipole moment approach. II. The 5400–11000 cm^{-1} region. JQSRT 2007;104:342–56.
[18] Oshika H, Toba A, Fujitake M, Ohashi N. Newly observed vibrational bands of N_2O in 1.3 μm region. J Mol Spectrosc 1999;179:324–5.
[19] Ni HY, Song KF, Perevalov VI, Tashkun SA, Liu AW, Wang L, et al. Fourier-transform spectroscopy of $^{14}N^{15}N^{16}O$ in the 3800–9000 cm^{-1} region and global modeling of its absorption spectrum. J Mol Spectrosc 2008;248:41–60.
[20] Bertseva E, Kachanov AA, Campargue A. Intracavity laser absorption spectroscopy of N_2O with a vertical external cavity surface emitting laser. Chem Phys Lett 2002;351:18–26.
[21] Ding Y, Perevalov VI, Tashkun SA, Teffo JL, Bertseva E, Campargue A. Weak overton transitions of N_2O around 1.05 μm by ICLAS-VECSEL. J Mol Spectrosc 2003;220:80–6.
[22] Bertseva E, Campargue A, Perevalov VI, Tashkun SA. New observations of weak overtone transitions of N_2O by ICLAS-VeCSEL near 1.07 μm. J Mol Spectrosc 2004;226:196–200.
[23] Song KF, Ni HY, Liu AW, Wang L, Hu SM. Fourier-transform spectroscopy of $^{15}N^{14}N^{16}O$ in the 3500–9000 cm^{-1} region. J Mol Spectrosc 2009;255:24–31.